Pergamon

Int. J. Heat Mass Transfer. Vol. 39, No. 9, pp. 1773–1783, 1996

0017-9310/96 $15.00+0.00

0017-9310(95)00297-9

Heat sinks with sloped plate fins in natural and forced convection

GUSTAVO LEDEZMA and ADRIAN BEJAN†

Department of Mechanical Engineering and Materials Science, Duke University, Durham, NC 27708-0300, U.S.A.

(*Received* 1 *June* 1995 *and in final form* 10 *August* 1995)

Abstract—This is an experimental and numerical study of natural convection and forced convection air cooling of plate finned heat sinks. The study documents quantitatively two effects: (1) the orientation of the fin array relative to the gravitational field in natural convection, and relative to a free stream in forced convection, and (2) the tilting of the crests of the plate fins relative to the approaching flow. In each configuration, the results based on complete three-dimensional numerical simulations of the flow and heat transfer confirm the validity of the results determined based on direct measurements. For example, it is shown that the overall thermal conductance of the heat sink increases when the fin crests are inclined so that they face the approaching fluid. This augmentation effect increases as the coolant velocity increases. The thermal performance of arrays positioned perpendicularly to the flow is also documented.

1. INTRODUCTION

Air cooling is recognized as an important technique in the thermal design of electronic packages. This technique promises to gain in importance because air is the most accessible coolant, and the methods based on it are simple and robust, particularly with respect to safe operation in hostile environments (contaminated air, vibrations, noise, humidity) [1]. These advantages stimulated considerable research on the development of optimization of finned heat sinks in both natural and forced convection. Reviews of the progress made in this field have been presented in refs. [2–4].

In a recent paper [5] it was suggested that the performance of an air heat sink with parallel plate fins can be improved by tilting the crests of the plate fins (e.g. Fig. 1). This suggestion was based on a simple two-dimensional model in which the local heat transfer coefficient h was assumed known from boundary layer theory. The fact that h becomes smaller downstream suggested that more fin material (a higher crest) should be placed downstream such that the overall heat transfer is augmented. That study was limited to forced convection. The authors also noted that their simple model breaks down when the fin slope is so large that the upstream height of the fin vanishes (e.g. array C, Fig. 2).

The objective of the present work was to investigate fully the heat transfer augmentation merits of tilting the crests of plate fins in air cooled heat sinks. We accomplished this objective in four complementary phases distinguished with respect to the heat transfer mechanism (natural vs forced convection) and the method (experiments vs numerical simulation). In the following material we document the results of these parallel investigations and the summarizing view that tilted crests are indeed a heat transfer augmentation feature worthy of attention.

2. NATURAL CONVECTION EXPERIMENTS

2.1. *Apparatus*

The experiments consisted of measuring the temperature at the base of a square package fitted with plate fins cooled by natural convection. The package and experimental apparatus are shown in Fig. 1. The plate-fin heat sink geometries tested are summarized in Fig. 2. These varied with respect to the inclination of the crest of the plate fins, and the orientation of the entire package.

With reference to the notation of Fig. 2, the fixed dimensions of the package are $L = 49$ mm, $t = 1$ mm, $B = 2$ mm and $W = 3$ mm. The fin-to-fin spacing W was selected such that its order of magnitude corresponds to the optimal spacing between vertical parallel plates of height L, namely $W_{opt} \sim 2L\,Ra_L^{-1/4}$ (e.g. refs. [6, 7]). The base plate thickness B was made thick enough to provide a uniform temperature distribution over the $L \times L$ area. The fin thickness t was chosen such that the fin efficiency was practically equal to 1, as in the experimental studies of refs. [8–10].

The fin crest inclination was varied by machining three model arrays: array A with $H_1 = H_2 = 15$ mm; array B with $H_1 = 7.5$ mm and $H_2 = 22.5$ mm; and array C with $H_1 = 0.75$ mm and $H_2 = 29.3$ mm. These three model arrays and positions 1, 2 and 3 (Fig. 2) allowed us to vary the crest inclination through five sequential values. In addition, we tested all the arrays

† Author to whom correspondence should be addressed.

NOMENCLATURE

A_b fin base area
A_s fin surfaces with convection
b fin crest slope parameter; equation (17)
B base thickness, Fig. 1
d, m, p, s computational domain dimensions, Fig. 7
g gravitational acceleration
H fin crest height, equation (17)
$\tilde{H}$ average crest height
$H_{1,2}$ fin edge dimensions, Fig. 1
k fluid thermal conductivity
k_s solid thermal conductivity
L side of square package, Fig. 1
Nu_L overall Nusselt number, equation (1)
p pressure
P dimensionless pressure, equation (9)
$\hat{P}$ dimensionless pressure, equation (25)
Pe Peclet number, equation (25)
Pr Prandtl number, ν/α
q power supplied to one fin
q'' heat flux through the fin base
q''_{avg} average heat flux through the fin surfaces with convection
R electric resistance
Ra_L Rayleigh number, equation (2)
Re_L Reynolds number, equation (8)
t fin thickness, Fig. 1
T temperature
T_∞ ambient temperature
$\tilde{T}$ dimensionless temperature, equation (9)
$\hat{T}$ dimensionless temperature, equation (19)
u, v, w velocity components
U, V, W dimensionless velocity components, equation (8)
$\hat{U}, \hat{V}, \hat{W}$ dimensionless velocity components, equation (25)
V_∞ free stream velocity
W fin spacing, Fig. 1
x, y, z coordinates
X, Y, Z dimensionless coordinates.

Greek symbols
α fluid thermal diffusivity
β coefficient of volumetric thermal expansion
μ viscosity
ν kinematic viscosity.

horizontally facing upward (position 4), and vertically with the fins running horizontally (position 5). The model arrays were made from a high thermal conductivity aluminum alloy. The volume (amount of metal) did not vary from one model array to the next, and since the plate fin thickness was fixed, the total heat transfer area did not vary either.

The base of the package consisted of a 5 mm thick insulating layer (balsa wood) and a thin thermofoil heater MINCO HR5417R5.3L12. The model array, heater and wood base were bonded together with aluminum clamps. The contact surfaces were covered with silicone heat sink compound to ensure good thermal contact. A variable autotransformer powered the heater, which has a resistance of 5 Ω.

The package was tested inside an enclosure with the dimensions 304 mm × 304 mm × 910 mm. The internal and external surfaces of the enclosure were covered with aluminum foil to minimize the effect of thermal radiation. The radiation contribution to the total heat transfer rate varied between 3 and 7%: this estimate is based on the procedure described in Rea and West [11], by taking into account the cavity effect of the U-shaped channels formed by the fins. The top and bottom ends of the enclosure were left open in order to prevent the stagnation and gradual warming of the trapped air.

2.2. *Procedure*

The temperature measured under the square base of the model array was almost uniform. This measurement was made in a preliminary run with six chromel–alumel thermocouples (0.4°C estimated accuracy) embedded in the base of the model array. The maximum difference between the six temperatures was 2% when the heater power varied such that the base temperature varied from 25 to 70°C.

The temperature measurements during the actual tests were made with precision thermistors of type YS44004, which were calibrated between 20 and 80°C. One thermistor was attached to the mid-point of the base of the model array. Another thermistor was located at the bottom of the enclosure to sense the ambient temperature. The heat transferred by conduction across the insulation layer varied between 4 and 11% of the total power dissipated in the heater. This estimate is based on the temperature difference measured across the insulation layer.

Each run was started by setting the power input to the heater, and waiting 2 h to make sure that no transients were present during the measurements. The actual measurements were made over approximately 30 min. Each of the points plotted in Figs 3–6 were obtained by conducting 25 runs at the same power setting, and averaging the measurements.

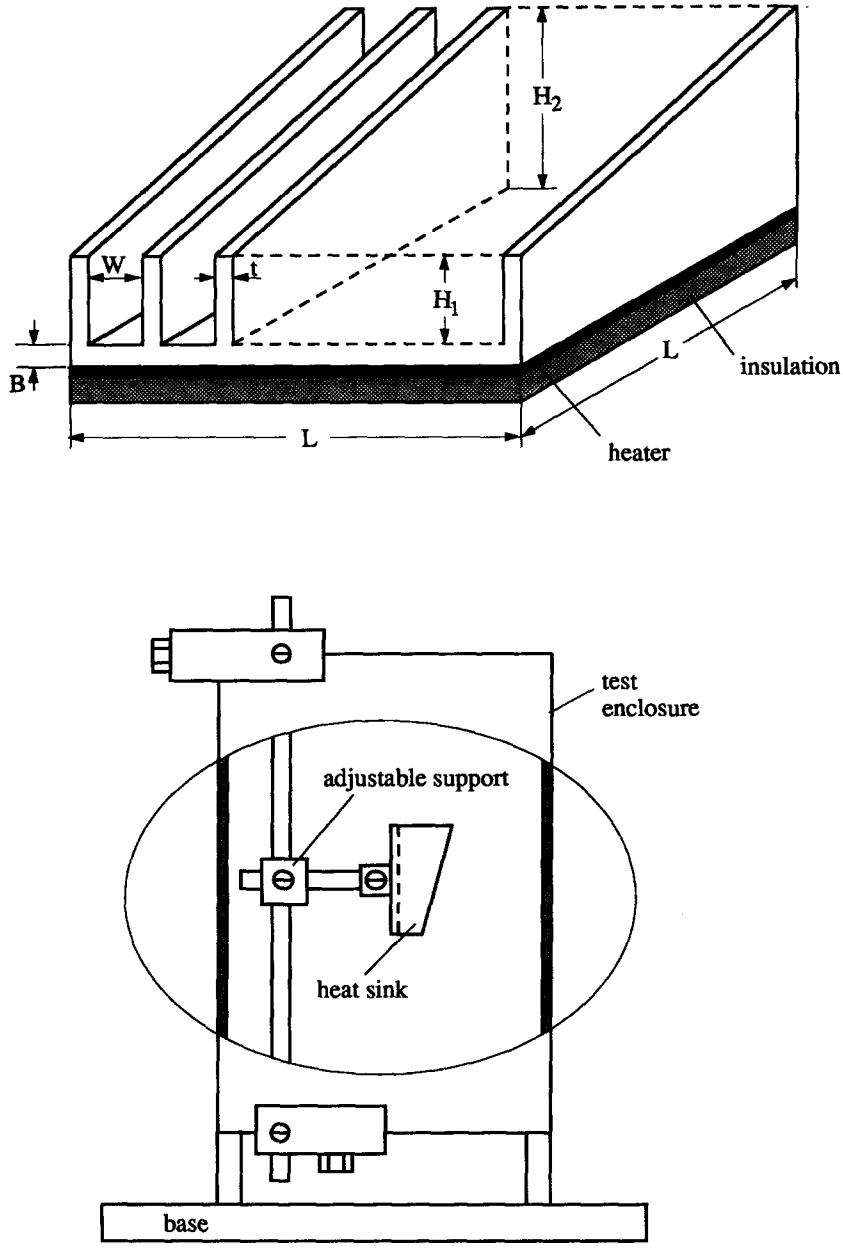

Fig. 1. Package with plate-fin heat sink, and experimental apparatus for natural convection cooling.

The experimental uncertainties were calculated using the root-sum-square method described by Moffat [12]. The uncertainty U_f in a quantity f has contributions due to the bias limit (B_f) or constant error, and the precision limit (P_f) or two times the standard deviation of the measurements: $U_f/f = [(P_f/f)^2 + (B_f/f)^2]^{1/2}$. The bias limit in the measurement of the temperature was (± 0.001 K): this was determined from the response of the thermistor and the 0.01 Ω resolution of the HP3468B multimeter used to read the resistance. The temperature bias limit was estimated under the least favorable conditions, which are when the base temperature of the model array is the highest (70°C). In this temperature range the calibration of the thermistors indicated that $dT/dR = -(1/14)$ K Ω^{-1}. The precision limit of the temperature difference was set equal to two times the standard deviation in each set of measurements. The bias limit of the thermal conductivity and apparent emittance of the insulation layer was taken as 20% of the reported values (0.037 W $(m \cdot K)^{-1}$ and, respectively, 0.5). The uncertainties in L, k, k_s and v are negligible. The only important contributions to the uncertainties in Ra_L and Nu_L are made by the measurement of the heat input to the thermofoil heater. The precision limit of the temperature difference is also negligible (± 0.2°C). This procedure led to an estimated maximum uncertainty of 6% in the Nusselt

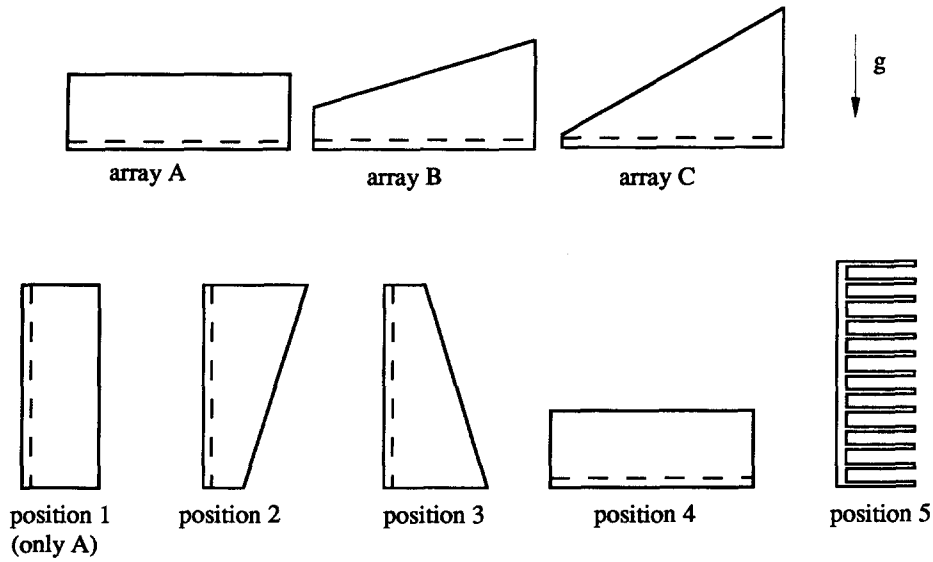

Fig. 2. The crest inclinations of the plate fins, and the positions of heat sinks tested.

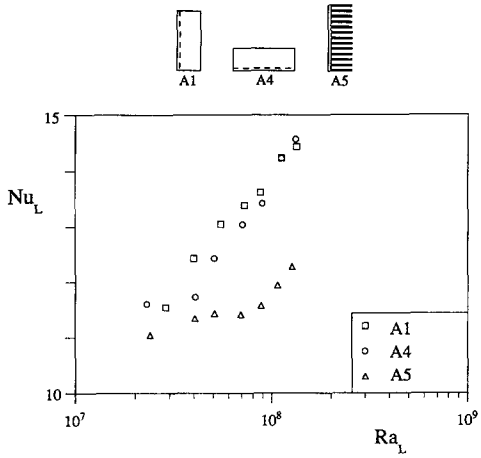

Fig. 3. Experimental results on the effect of Ra_L and the orientation of array A.

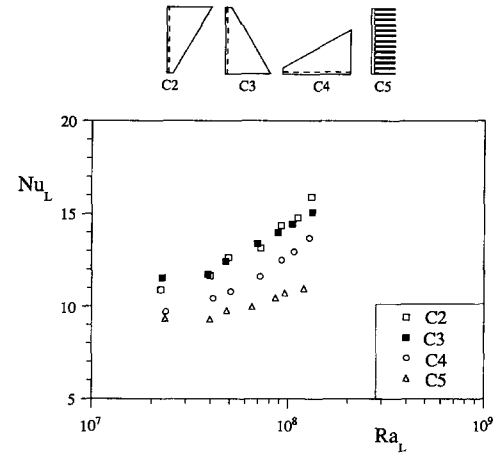

Fig. 5. Experimental results on the effect of Ra_L and the orientation of array C.

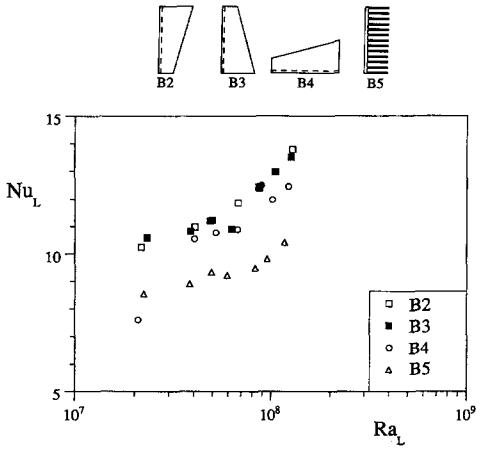

Fig. 4. Experimental results on the effect of Ra_L and the orientation of array B.

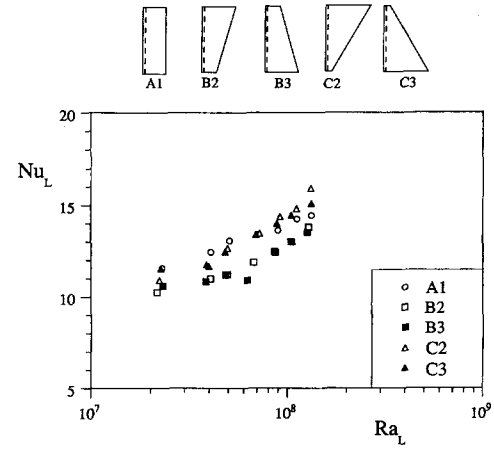

Fig. 6. Vertical arrays with vertical fins: the effect of Ra_L and the inclination of the fin crest.

number of equation (1), and 3% in the non-dimensional temperature $\tilde{T}$ defined by equation (9).

2.3. *Results*

There are three separate effects that are documented by the experimental results collected in this study, namely the effects associated with changing the Rayleigh number, the orientation of the model array, and the inclination of the fin crest. The first two effects are shown in Figs. 3–6, while the crest inclination effect is left for Figs. 8 and 9, where it will be discussed in relation to the corresponding results generated by numerical simulations.

The overall thermal conductance or Nusselt number is defined by

$$Nu_L = \frac{q'' L A_b / A_s}{k(T - T_\infty)}, \tag{1}$$

where q''_{avg} is the average heat flux through the fin surfaces with convection, $q''_{avg} A_s = q'' A_b$. The Rayleigh number is based on the uniform heat flux q'', which is generated by the thin-film heater,

$$Ra_L = \frac{g\beta q'' L^4}{\alpha \nu k}. \tag{2}$$

To start with, in Fig. 3 we see the effect of changing the position of array A. Although the vertical position (A1) is relatively the best, its Nu_L values are nearly the same as those measured while holding the array horizontally (A4). The thermal conductance is between 10 and 20 percent smaller when the array is vertical and the fins horizontal (A5). In position A5, the Ra_L effect on Nu_L is not as strong as in positions A1 and A2.

The results corresponding to arrays B and C are reported in Figs. 4 and 5. Once again the highest Nu_L values are associated with arrays and fins that are oriented vertically. The performance of horizontal arrays facing upward (B4, C4) is only slightly inferior. The vertical arrays with horizontal fins (B5, C5) are characterized by Nu_L values that fall noticeably below those of the other orientations.

The new aspect of a series of tests such as Fig. 4 or Fig. 5 is that by comparing B2 with B3, or C2 with C3, we can see the effect of changing the orientation of the sloped fin. Both figures show that the effect of turning the vertical array upside-down is negligible within the uncertainties of the measurements. The same conclusion is revealed by Fig. 6, which summarizes all the results obtained with vertical arrays and vertical fins. An exception is one Nu_L point for B3 in Fig. 4, which falls by about 10% under the corresponding point for B2: this small difference may be due to flow separation or transition to turbulence near $Ra_L \sim 10^8$. The B4 and B5 data in the same figure show a clear change in their alignment near that Rayleigh number.

Figure 6 also shows the effect of changing the slope of the fin crest, which was the original motivation for conducting this study. We see that the array with the most severe crest inclination (array C) has a higher Nu_L than an array with moderate crest inclination (array B). It is interesting, however, that when the crest inclination is absent (array A) the Nu_L values are comparable to those associated with array C. This finding and, in general, the effect of tilting the fin crest served as a stimulus for conducting a numerical study of the same natural convection configuration. Figure 6 also shows that configurations B2 and C2 perform better at higher Rayleigh numbers: this brings up the question of whether the crest slope should be optimized for the specified Ra_L of a given application.

3. NATURAL CONVECTION NUMERICAL STUDY

3.1. *Model*

The domain in which we calculated the flow and temperature fields is shown in Fig. 7. It consists of half of one fin and a large enough space around the fin. It was sufficient to consider only one fin because in the experiments the spacing between fins was about twice as large as the thickness of one thermal boundary layer, in accordance with the rule for selecting the optimal spacing for maximum overall thermal conductance. This means that each fin is lined vertically by its own boundary layer, which does not merge with the boundary layers of the adjacent fin.

The numerical model consisted of coupling the external natural convection to the conduction heat transfer in the solid. The conservation of mass momentum and energy in the fluid,

$$\frac{\partial U}{\partial X} + \frac{\partial V}{\partial Y} + \frac{\partial W}{\partial Z} = 0 \tag{3}$$

$$U\frac{\partial U}{\partial X} + V\frac{\partial U}{\partial Y} + W\frac{\partial U}{\partial Z} = PrRa_L^{-2/5}\left(-\frac{\partial P}{\partial X} + \nabla^2 U\right) \tag{4}$$

$$U\frac{\partial V}{\partial X} + V\frac{\partial V}{\partial Y} + W\frac{\partial V}{\partial Z} = PrRa_L^{-2/5}\left(-\frac{\partial P}{\partial Y} + \nabla^2 V\right) + Pr\tilde{T} \tag{5}$$

$$U\frac{\partial W}{\partial X} + V\frac{\partial W}{\partial Y} + W\frac{\partial W}{\partial Z} = PrRa_L^{-2/5}\left(-\frac{\partial P}{\partial Z} + \nabla^2 W\right) \tag{6}$$

$$U\frac{\partial \tilde{T}}{\partial X} + V\frac{\partial \tilde{T}}{\partial Y} + W\frac{\partial \tilde{T}}{\partial Z} = Ra_L^{-2/5}\nabla^2 \tilde{T} \tag{7}$$

are based on assuming a fluid with nearly constant properties, and a density–temperature relation represented by the Boussinesq approximation. The dimensionless variables are defined by

$$(X, Y, Z) = \frac{(x, y, z)}{L} \quad (U, V, W) = \frac{(u, v, w)}{(\alpha/L)Ra_L^{2/5}} \tag{8}$$

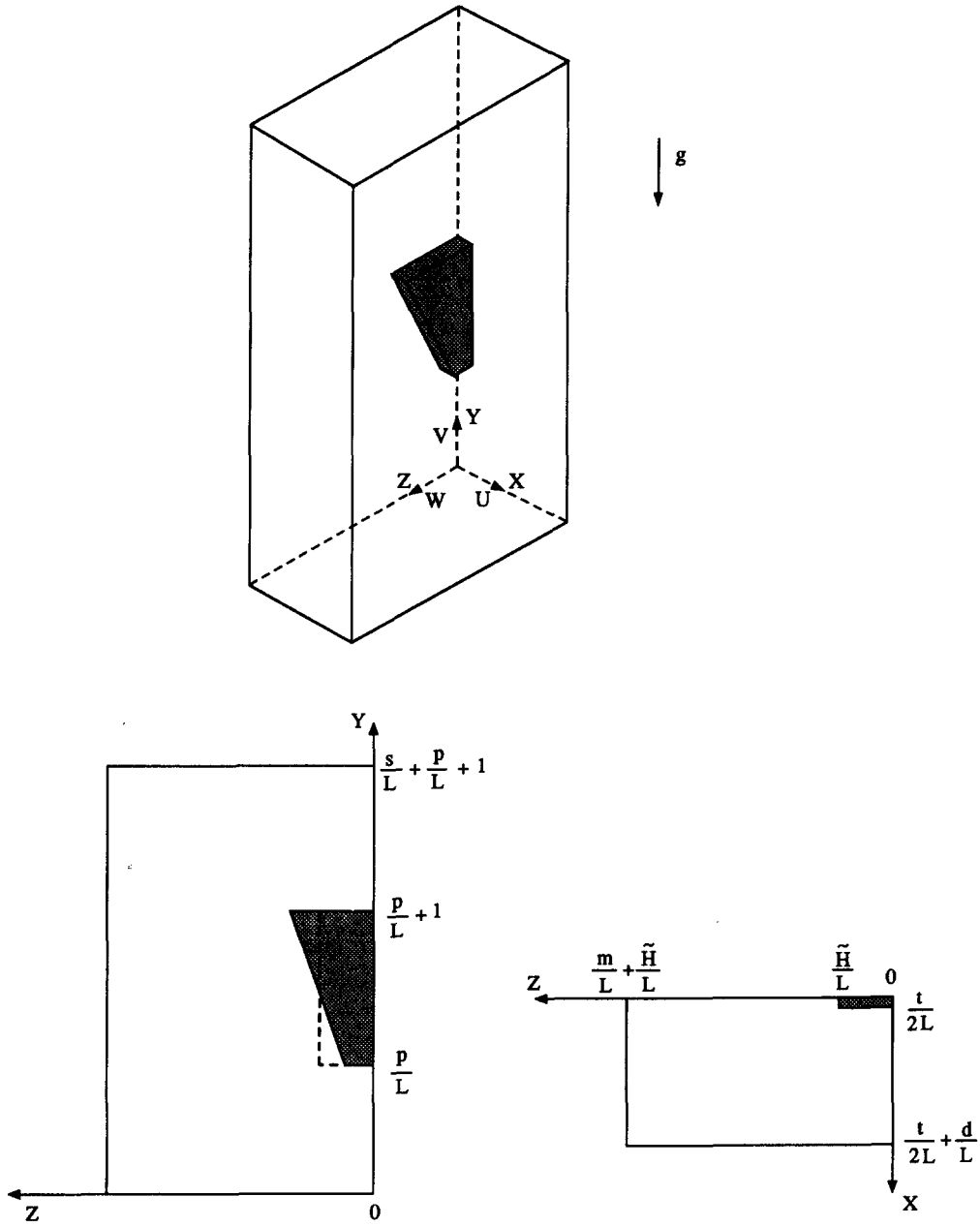

Fig. 7. The computational domain and the relative position of the half-fin with inclined crest.

$$P=\frac{pL^2}{\mu\alpha Ra_L^{2/5}} \quad \tilde{T}=\frac{T-T_\infty}{(q''/k)L}Ra_L^{1/5}. \tag{9}$$

The corresponding energy equation for conduction in the solid is

$$\nabla^2\tilde{T}=0. \tag{10}$$

The boundary conditions are

$$U=0 \quad \frac{\partial V}{\partial X}=0 \quad \frac{\partial W}{\partial X}=0 \quad \text{at} \quad X=0 \tag{11}$$

$$U=0 \quad V=0 \quad W=0 \quad \text{at} \quad Y=0 \tag{12}$$

$$W=0 \quad \text{at} \quad Z=0 \quad \text{and} \quad Z=m/L+\tilde{H}/L \tag{13}$$

$$\tilde{T}=0 \quad \text{at} \quad Y=0 \tag{14}$$

$$\frac{\partial\tilde{T}}{\partial Z}=-1 \quad \text{at} \quad Z=0 \quad 0\leqslant X\leqslant t/2L$$

and

$$p/L\leqslant Y\leqslant(p+L)/L \tag{15}$$

$$\frac{\partial\tilde{T}}{\partial Z}=0 \quad \text{at} \quad Z=0 \quad \text{around the fin base.} \tag{16}$$

The crest of the plate fin was located at the distance H in the z direction,

$$H(y) = \tilde{H}\left[1 + b\left(\frac{y}{L} - \frac{1}{2}\right)\right], \qquad (17)$$

where $\tilde{H}$ is the average crest height and b is the dimensionless crest slope. Additional boundary conditions are zero shear and zero heat flux around the periphery of the computational domain, and no-slip on the fin surfaces in contact with fluid. The lateral boundary $X = (t/2L) + d/L$ was located far enough from $X = 0$ such that specifying zero heat flux on this boundary led to the same results as specifying $\tilde{T} = 0$. The results presented in this paper were obtained using $d/L = 0.59$. The nondimensionalized conditions for the conservation of heat flow through the solid–fluid interfaces (not shown) contain the solid–fluid thermal conductivity ratio k_s/k. This ratio was set equal to 6150, which corresponds to the aluminum–air combination used in the experiments.

3.2. *Method*

Equations (3)–(10) were solved using a finite element code [13]. The domain was discretized nonuniformly using isoparametric brick elements with eight nodes. The velocity components and temperatures were approximated using trilinear interpolation functions. The method to solve the nonlinear equation from the Galerkin finite element procedure consisted of a fixed point iteration and a quasi-Newton Broyden update scheme. The pressure was eliminated based on a penalty function approach with an error factor of 10^{-6}. The coupled fluid and temperature solution required approximately 700 s for each run on the CRAY Y-MP of the North Carolina Supercomputer Center. The high Ra_L solutions that were developed from lower Ra_L solutions required between 150 and 400 s.

The results were generated using a mesh with 3216 elements. Accuracy tests were conducted to guarantee that the solution is mesh independent. The mesh density was increased by 60% (from 3216 to 5336 elements) such that the new elements were added uniformly throughout the domain. The corresponding change in the maximum $\tilde{T}$ value at the fin surface was found to be less than 1%.

Additional tests showed that the size of the computational domain ($m/L = 1.25, p/L = 0.5, s/L = 0.6$) is large enough such that additional increases in these ratios lead to changes smaller than 0.6% in $\tilde{T}_{max}$. This was done by increasing one side of the domain and holding the other side fixed: s/L was increased by a factor of 2, and m/L by a factor of 1.6. These tests were performed for $Ra_L = 10^6$ and 10^7 in the configuration were the crest was not tilted ($b = 0$).

3.3. *Results*

The numerical results were developed in two phases. In the first, we used the numerical model to verify the results obtained experimentally, and to test the model itself (Fig. 8). In the second phase we generated numerically the overall thermal conductance Nu_L as a function of Ra_L and the crest slope b (Fig. 9). The Prandtl number was set at $Pr = 0.72$ in all cases.

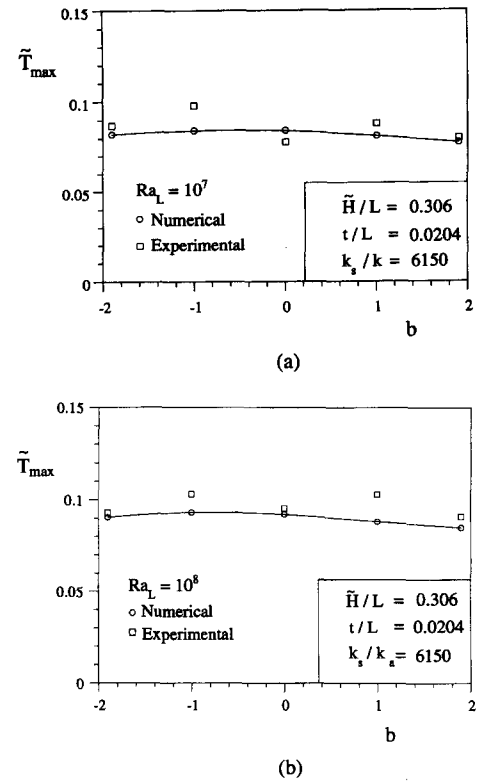

Fig. 8. The effect of fin crest slope (b) on the maximum temperature along the fin base.

Figure 8 shows the effect of the crest inclination, and a comparison between the numerical and experimental results for the plate fin dimensions used in the experiments. For the numerical results, the ordinate shows the maximum temperature that occurs along the fin base. The agreement between the two sets of data is good, especially in view of the fact that in the experiments the fins and the heater were separated by a conducting slab of thickness B (Fig. 1), which made the base of the fin isothermal. That slab is absent in

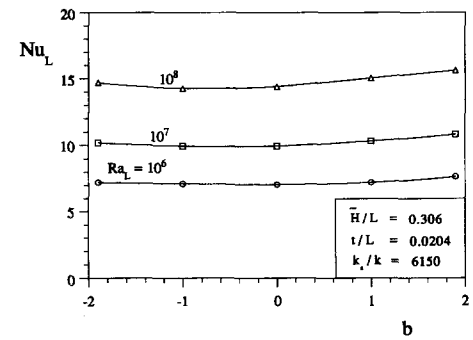

Fig. 9. The effect of Rayleigh number and fin crest slope on the overall Nusselt number.

the numerical model (Fig. 7), hence the nonuniform temperature over the fin base.

Another conclusion drawn from the numerical results is that the most effective heat sink is the one with fin crests that have the largest positive slope b. In the experiments this would correspond to a geometry such as array C in position 2. Interpolating between the numerical results for $b = 0$ and $b = -1$ we find that the least effective crest inclination is roughly $b = -0.5$. The experimental data show a similar b effect on $\tilde{T}_{max}$, the exception being case $b = 0$ which falls below the expected peak of the curve. We believe that this anomaly is due to the fact that the heat losses through the leading and trailing faces of the fins are larger when those faces are *both* sizable, namely of order H_{avg} as in the case of array A in position 1.

Figure 9 summarizes the numerical results obtained in the Ra_L range 10^6–10^8, as b increases from -1.9 to 1.9. The results are reported as the overall Nusselt number, which is based on equation (1) in which the base temperature was set equal to the maximum temperature. This figure shows that although the effect of b is weak the trend is such that the importance of b increases as the Rayleigh number increases.

4. FORCED CONVECTION EXPERIMENTS

The sequence of experiments and numerical simulations described in Sections 2 and 3 was repeated for forced convection. Because of the similarities between the two sequences, the description of the forced convection work is abbreviated.

The forced convection experiments were performed in a low speed, suction-type wind tunnel with a flow cross-section of 122×130 mm and test section length of 584 mm, Fig. 10. The air speed was regulated using a variable autotransformer connected to a fan. Experiments were performed at three different air velocities that correspond to the Reynolds numbers $Re_L = 3750$, 6000 and 7200, where

$$Re_L = \frac{V_\infty L}{\nu}. \tag{18}$$

The mean velocity in the test section was measured with a Taylor anemometer, which was placed inside the tunnel 10 times for periods of 45 min in each case. The average air speed was calculated as the displacement measured by the anenometer divided by the time. In this way we estimated the power required to achieve a certain air speed. The bias limit of the mean velocity was $\pm 5\%$.

The temperature at the base of each array was measured with four thermistors attached as shown in Fig. 10, where the dimensions are indicated in millimeters. An additional thermistor was placed upstream to monitor the free stream temperature. The heat loss through the insulation plate (Fig. 1) was negligible. We measured it by attaching thermistors on both sides of the insulation plate, and found that when $Re_L = 3750$ the heat transfer through the insulation plate is less than 0.1% of the heat generated by the film heater.

After the start of each run, we monitored the thermistor readings and the power input to the heater for 2 h, to be certain that the experiment reached the steady state. The measurements were made over a period of 45 min for each case. A total of 25 thermistor readings were taken from each run; later these readings were averaged. The precision limit of the temperature was taken as equal to twice the standard deviation in the measurements. The new dimensionless temperature $\hat{T}$ is defined by

$$\hat{T} = \frac{T - T_\infty}{q/(kt)}. \tag{19}$$

In the calculation of the uncertainties, we found that the contribution of the bias limit of the temperatures is negligible due to the use of thermistors. The uncertainty in the air speed measurement is the only significant contribution to the uncertainty in the Reynolds number. The maximum uncertainties in the reported Re_L and $\hat{T}$ values are 5 and 10%, respectively.

Once again, the focus of the experiments was on determining the effect of the crest slope b on the maximum temperature measured along the fin base. Figure 11a–c shows an example ($Re_L = 7200$) of how the base temperature varies with b and the longitudinal position in the flow direction (namely, direction Y in Fig. 7). The maximum temperature $\hat{T}_{max}$ was determined after curve-fitting the three ($\hat{T}$, Y) data. The cases indicated with b values (0, ± 1, ± 1.9) refer to arrays A, B and C oriented such that the plate fins and the base are parallel to the air stream. The 'vertical array' refers to array A positioned vertically in the middle of the air channel, with the fins facing the incoming stream. It is interesting that placing the array perpendicular to the air stream has the effect of reducing the base temperature by 10–20% relative to when the fin-to-fin channels are swept longitudinally by the flow. In the latter, $\hat{T}$ tends to increase in the flow direction reaching its highest value in the downstream half of the swept length.

The maximum temperatures are summarized in Fig. 12a–c, which shows the effect of changing the slope of the fin crest and the Reynolds number. These data refer only to arrays oriented with the fin-to-fin channels parallel to the free stream. As in natural convection, the lowest $\hat{T}_{max}$ values belong to the array with the largest slope b, namely array C oriented such that the tilted roof of the array looks at the approaching stream. There is a reduction of almost 20% in $\tilde{T}_{max}$ when b changes from 0 to 1.9 at $Re_L = 7200$.

5. FORCED CONVECTION NUMERICAL STUDY

The numerical simulation of the flow and heat transfer was based on the same method as the one described in Section 3.2. The free stream was always

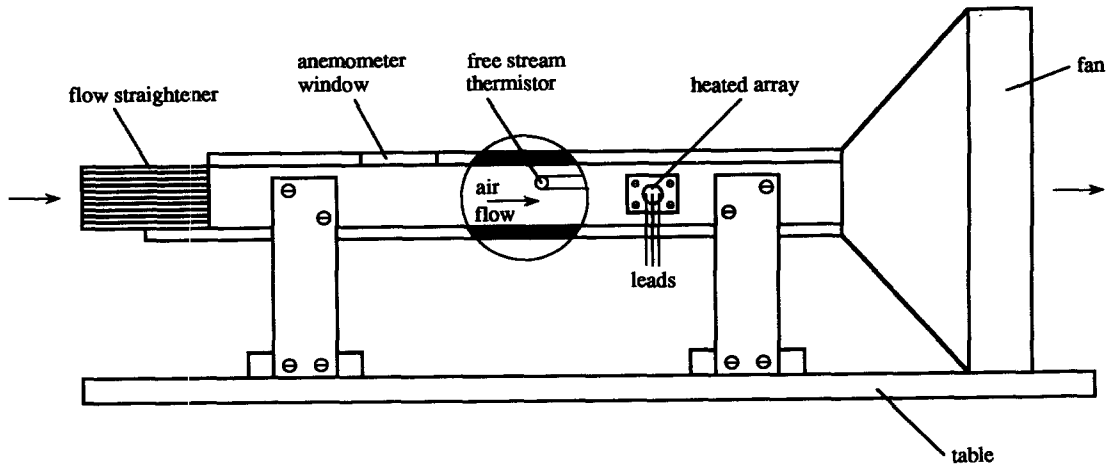

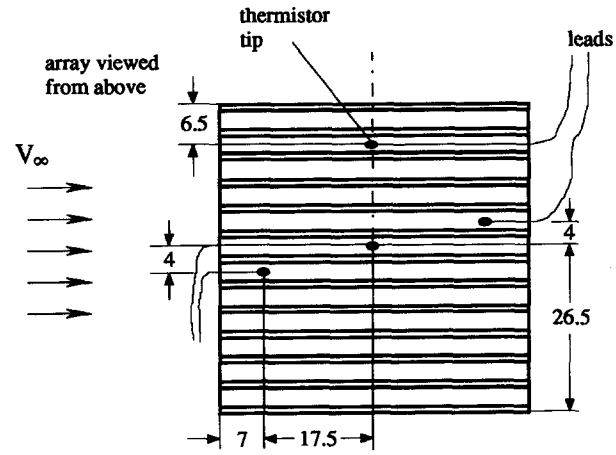

Fig. 10. The wind tunnel for the forced convection experiments, and the thermistor arrangement.

aligned with the direction shown as Y in Fig. 7, i.e. parallel to the channels formed between fins. The equations for mass, momentum and energy in the fluid are

$$\frac{\partial \hat{U}}{\partial X}+\frac{\partial \hat{V}}{\partial Y}+\frac{\partial \hat{W}}{\partial Z}=0 \tag{20}$$

$$\hat{U}\frac{\partial \hat{U}}{\partial X}+\hat{V}\frac{\partial \hat{U}}{\partial Y}+\hat{W}\frac{\partial \hat{U}}{\partial Z}=-\frac{\partial \hat{P}}{\partial X}+\frac{1}{Re_L}\nabla^2\hat{U} \tag{21}$$

$$\hat{U}\frac{\partial \hat{V}}{\partial X}+\hat{V}\frac{\partial \hat{V}}{\partial Y}+\hat{W}\frac{\partial \hat{V}}{\partial Z}=-\frac{\partial \hat{P}}{\partial Y}+\frac{1}{Re_L}\nabla^2\hat{V} \tag{22}$$

$$\hat{U}\frac{\partial \hat{W}}{\partial X}+\hat{V}\frac{\partial \hat{W}}{\partial Y}+\hat{W}\frac{\partial \hat{W}}{\partial Z}=-\frac{\partial \hat{P}}{\partial Z}+\frac{1}{Re_L}\nabla^2\hat{W} \tag{23}$$

$$\hat{U}\frac{\partial \hat{T}}{\partial X}+\hat{V}\frac{\partial \hat{T}}{\partial Y}+\hat{W}\frac{\partial \hat{T}}{\partial Z}=\frac{1}{Pe}\nabla^2\hat{T}, \tag{24}$$

where (X, Y, Z) are given by equation (8) and

$$(\hat{U},\hat{V},\hat{W})=\frac{(u,v,w)}{V_\infty}\quad \hat{P}=\frac{p}{\rho V_\infty^2}\quad Pe=\frac{V_\infty L}{\alpha}. \tag{25}$$

The equation for conduction in the solid is $\nabla^2\hat{T}=0$. The boundary conditions are the same as in equations (12)–(17), except that the flow entrance condition (11) is replaced now by

$$\hat{U}=0\quad \hat{V}=1\quad \hat{W}=0\quad \text{at}\quad Y=0 \tag{26}$$

and, in addition, $\hat{U}=0$ at $X=t/2L+d/L$.

The computational domain is shown in Fig. 7, which can be imagined rotated by 90° clockwise to agree with the actual orientation of the flow in Fig. 10. The outer dimensions of the domain are $d/L=0.215$, $m/L=0.694$, $p/L=0.5$ and $s/L=1.5$. The inner dimensions were selected to agree with the dimensions of the arrays tested in the wind tunnel, namely,

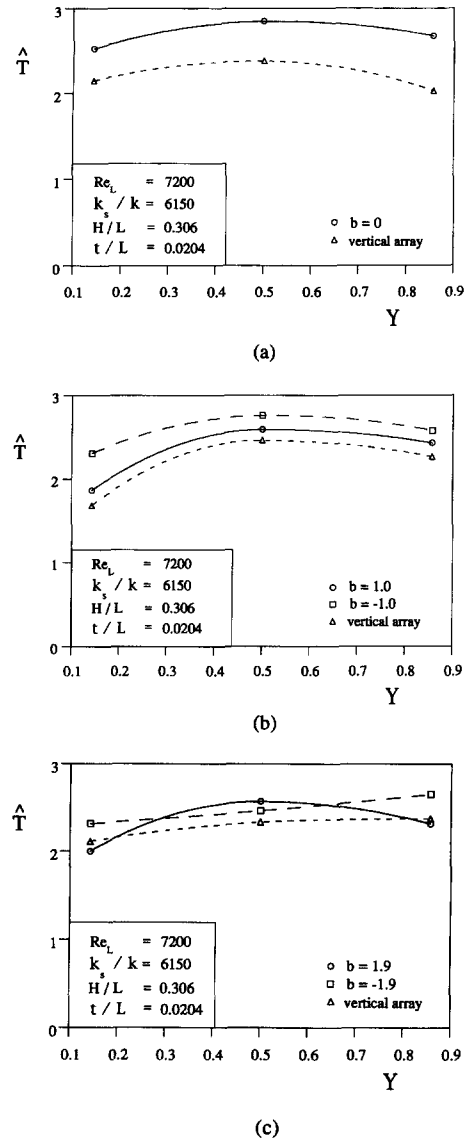

Fig. 11. The temperature distribution along the fin base and the effect of the slope b and the array orientation.

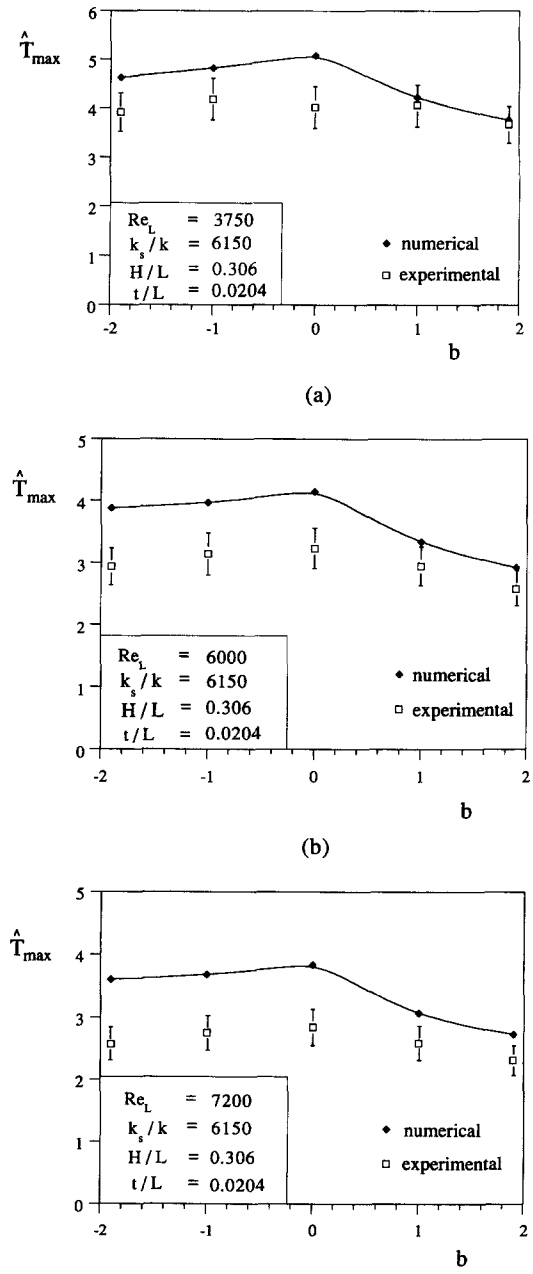

Fig. 12. Experimental and numerical results for the maximum base temperature during cooling by forced convection.

$\hat{H}/L = 0.306$ and $t/2L = 0.0102$. Numerical results were generated using a mesh with 6112 elements. This mesh was fine enough because $\hat{T}_{max}$ changed by less than 1.5% when the number of elements was increased uniformly from 6112 to 8216. The outer dimensions of the computational domain were selected based on a similar test: the relative change in $\hat{T}_{max}$ was less than 1.5% when s/L and d/L were increased by a factor of 1.3.

It is worth stressing that the single fin model does not capture all the flow and heat transfer features of a plate-fin sink exposed to a free-stream. A portion of the actual flow is diverted over the crests of the plate fins, while another portion flows around the sides [14]. These features are primarily responsible for the differences that we found between the numerical and experimental results for the same configuration. The single fin model was chosen for its simplicity, and in order to focus closely on the effect of tilting the crest. The numerical simulations were not designed to reproduce (duplicate) quantitatively the experimental results: their purpose was to provide an alternative—another set of eyes—for viewing the trends, i.e. how the performance responds to changes in the design. Such an alternative strengthens the conclusions reached experimentally, and, at the same time, provides a more flexible and less expensive method of

examining large numbers of geometrically different designs.

Figure 12a–c shows that the numerical results for $\hat{T}_{max}$ follow the same trend as the results obtained experimentally. The effect of the slope parameter b developed numerically is more accentuated than the experimental one, for example, if fin shape is changed from $b = 0$ to $b = 1.9$ the maximum temperature experiences a drop of approximately 30%. This drop is accentuated further as the Reynolds number increases.

6. CONCLUSION

The summarizing conclusion of this experimental and numerical study is that tilting the crests of air cooled plate fins has a measurable effect on the overall thermal conductance of the heat sink. For the practitioner, however, this effect may not be sufficiently pronounced to justify additional complications and cost of manufacturing. Calculations based on complete (three-dimensional) numerical simulations of the flow and temperature field around the heat sink agree with the results based on laboratory measurements. Furthermore, the experimental and numerical results obtained for forced convection cooling reinforce the trends revealed by the corresponding results for natural convection.

In brief, the best plate fins are those with crests tilted such that their tops face the approaching flow. The augmentation effect associated with tilting the crests increases as the air flow increases, for example, in switching from natural to forced convection, or increasing Re_L in forced convection. We also documented the performance of plate finned heat sinks oriented perpendicularly to the flow, in both forced convection and in natural convection.

Acknowledgements—This work was supported in part by IBM Corporation, Research Triangle Park, under the guidance of Dr Sang W. Lee. The computational work was supported by a grant from the North Carolina Supercomputing Center. We owe special thanks to Professor Dan G. Cacuci of Karlsruhe University for helping us with the design and high precision machining of the arrays tested in the experiments.

REFERENCES

1. R. C. Chu, Recent development of computer cooling technology, Keynote Paper, *6th International Symposium Transport Phenomena Thermal Engineering* (ISTP-6), Seoul (1993).
2. A. D. Kraus, Sixty-five years of extended surface technology 1922–1987, *Appl. Mech. Rev.* **41**, 321–364 (1988).
3. F. P. Incropera, Convection heat transfer in electronic equipment cooling, *J. Heat Transfer* **110**, 1097–1111 (1988).
4. A. Aziz, Optimum dimensions of extended surfaces operating in a convective environment, *Appl. Mech. Rev.* **45**, 155–173 (1992).
5. M. Morega and A. Bejan, Plate fins with variable thickness and height for air-cooled electronic modules, *Int. J. Heat Mass Transfer* **37**, Suppl. 1, 433–445 (1994).
6. N. K. Anand, S. H. Kim and L. S. Fletcher, The effect of plate spacing on free convection between heated parallel plates, *J. Heat Transfer* **114**, 515–518 (1992).
7. A. Bejan, *Heat Transfer*, pp. 394–395. Wiley, New York (1993); also in A. Bejan, *Convection Heat Transfer*, p. 157, problem 11. Wiley, New York (1984).
8. W. Nakayama, H. Matsushima and P. Goel, Forced convective heat transfer from arrays of finned packages. In *Cooling Technology for Electronic Equipment* (Edited by W. Aung), pp. 195–210. Hemisphere, New York (1988).
9. H. Matsushima, T. Yanagida and Y. Kondo, Algorithm for predicting the thermal resistance of finned LSI packages mounted on a circuit board, *Heat Transfer Jap. Res.* **21**, 504–517 (1992).
10. A. Karagiozis, G. D. Raithby and K. G. T. Hollands, Natural convection heat transfer from arrays of isothermal triangular fins in air, *J. Heat Transfer* **116**, 105–111 (1994).
11. S. N. Rea and S. E. West, Thermal radiation from finned heat sinks, *IEEE Trans. Parts, Hybrids, Packaging* **PHP-12**, 115–117 (1976).
12. R. J. Moffat, Describing the uncertainties in experimental results, *Experim. Therm. Fluid Sci.* **1**, 3–17 (1988).
13. FIDAP, *Theory Manual*, V. 7.0. Fluid Dynamics International, Evanston, IL (1993).
14. A. M. Morega, A. Bejan and S. W. Lee, Free stream cooling of a stack of parallel plates, *Int. J. Heat Mass Transfer* **38**, 519-531 (1995).